materials

MDPI

Article

Corrosion Performance of Nano-ZrO_2 Modified Coatings in Hot Mixed Acid Solutions

Wenhua Xu [1,2], Zhenyu Wang [1,*], En-Hou Han [1], Shuai Wang [1] and Qian Liu [1,3]

1 Key Laboratory of Nuclear Materials and Safety Assessment, Institute of Metal Research, Chinese Academy of Sciences, Shenyang 110016, China; whxu13b@imr.ac.cn (W.X.); ehhan@imr.ac.cn (E.-H.H.); shuaiwang@imr.ac.cn (S.W.); qliu17s@imr.ac.cn (Q.L.)
2 University of Chinese Academy of Sciences, Beijing 100049, China
3 School of Materials Science and Engineering, University of Science and Technology of China, Hefei 230026, China
* Correspondence: zzyywang@imr.ac.cn; Tel.: +86-24-2389-0525

Received: 5 May 2018; Accepted: 30 May 2018; Published: 1 June 2018

Abstract: A nano-ZrO_2 modified coating system was prepared by incorporation of nano-ZrO_2 concentrates into phenolic-epoxy resin. The corrosion performance of the coatings was evaluated in hot mixed acid solution, using electrochemical methods combined with surface characterization, and the effects of nano-ZrO_2 content were specially focused on. The results showed that 1% and 3% nano-ZrO_2 addition enhanced the corrosion resistance of the coatings, while 5% nano-ZrO_2 addition declined it. The coating with 3% nano-ZrO_2 presented the minimum amount of species diffusion, the lowest average roughness (5.94 nm), and the highest C/O ratio (4.55) and coating resistance, and it demonstrated the best corrosion performance among the coating specimens.

Keywords: nano coatings; EIS; corrosion performance; acid corrosion

1. Introduction

The flue gas from oxy-fuels has higher levels of acid gases, mainly including SOx and NOx with smaller amounts of HF and HCl [1]. The hot flue gases may be compressed and cooled to form mixed acid environments, which are mainly composed of highly concentrated H_2SO_4, HNO_3, HCl and HF. With pH values that are usually in the range of 0–2, the mixed acids environment promotes an extremely high rate of steel corrosion, threatening the safety and operation of equipment.

Organic coatings have been used to control the corrosion of steels in the highly acidic environment. Phenolic-epoxy resin is the most important and industrialized epoxy polymer and possesses excellent acid and alkali resistance [2,3]. It acts as a physical barrier layer between the metal substrate and solution to inhibit the permeation of water and aggressive ions [4]. However, aggressive ions can easily attack coatings through the pores, especially strong acid ions. Due to the presence of porosity [5] and inherent brittleness [6], many coatings used in these conditions are too intolerant for strong acid at high temperature, which leads to premature failure [7].

In recent years, nanoparticles in the coating systems have shown outstanding properties, i.e., excellent barrier resistance, flame retardancy, and wear resistance, etc. [8–12], which have attracted more and more attention. The barrier properties of the organic coatings can be improved by the inclusion of proper fillers, and nano-sized fillers have superior barrier properties than conventional fillers, even at low concentrations, due to their higher surface area [13]. Among these nanoparticles, ZrO_2 nanoparticles are one of the most promising types of pigment [14] because of its advantages, such as remarkable chemical stability, wear resistance, strength and fracture toughness, and chemical

resistance to extreme environments [15,16]. However, very few studies of organic coatings modified by nano-ZrO_2 in hot mixed acid have been reported.

In the present work, nano-ZrO_2-modified coatings are formulated to protect steel components in the acid industrial environment. The open circuit potential method (OCP), electrochemical impedance spectra (EIS), X-ray photoelectron spectroscopy (XPS), scanning electron microscopy (SEM), transmission electron microscopy (TEM), atomic force microscopy (AFM) and Raman spectra are utilized to characterize the effect of nano-ZrO_2 content on the corrosion resistance of composite coatings in mixed acid solution (including 3 wt % H_2SO_4, 1 wt % HCl, 0.5 wt % HNO_3, and 0.2 wt % HF) at 60 °C, which simulates the acidic environment in petrochemical plants. An anticorrosion mechanism of composite coatings is also proposed.

2. Materials and Methods

2.1. Sample Preparation

Phenolic-epoxy resin (epoxide equivalent per weight: 172–179 g/eq, viscosity (51.7 °C): 1100–1700 mPa·s, and density (25 °C): 1.21 g/mL, Sinopharm Chemical Reagent Co. Ltd., Shanghai, China), phenolic modified aromatic amine (HN01) (amine value: 290 ± 10 KOH mg/g, viscosity (25 °C): 960 mPa·s, and activated hydrogen equivalent per weight: 86, Sinopharm Chemical Reagent Co. Ltd., Shanghai, China) and ZrO_2 (type: HTZr-02, purity ≥ 90, grain size: 40 nm, surface area ≥ 20 m^2/g, and crystal form: tetragonal phase, Xiaohuang Nano Technology Co. Ltd., Shanghai, China) were used in this study. Propylene glycol methyl ether acetate (PMA), BYK106 dispersant, KH550 silane coupling agent, 240 mesh glass flake and other chemicals were from Shanghai Lingfeng Chemical Corp., Shanghai, China.

2.2. Preparation of Nano-ZrO_2 Concentrates

Nano-ZrO_2 particles were dried in a vacuum at 120 °C for 72 h before use. Twenty-three percent PMA and 10% BYK106 dispersant were charged into a flask. The mixture was dispersed for 10 min by high speed stirring, and then 67% nano-ZrO_2 powders were slowly added into it. The new mixture was kept on high speed stirring for another 30 min, and centrifuged for 2 min. Finally, the mixture was ground for 3 h in a ball mill to obtain nano-ZrO_2 concentrates.

2.3. Preparation of Nano-ZrO_2-Modified Coatings

Sixty-five percent phenolic-epoxy resin, 0.5% KH550 silane coupling agent, 34.1% 240 mesh flake, and 0.4% BYK106 dispersant were mixed and ground for 8 h in a ball mill to obtain the Z-0 coating. Furthermore, 1.49%, 4.48%, and 7.46% nano-ZrO_2 concentrates (namely 1%, 3% and 5% nano-ZrO_2) were incorporated into the Z-0 coating and the nano-ZrO_2-modified coatings, Z-1, Z-3 and Z-5, were produced. Four coatings were spread to one side of the 50 mm × 50 mm Q235 steel plates, and the coated plates were dried at room temperature for 48 h and then 50 °C for 5 h. The coating thickness was 80 ± 5 μm and was used for the EIS test. The composition of the coatings is listed in Table 1.

Table 1. Composition of coatings.

Sample Coding [1]	Composition
Coating Z-0	65% phenolic-epoxy resin, 0.5% KH550 silane coupling agent, 34.1% 240 mesh glass flake, 0.4% BYK106 dispersant, 30% HN01 curing agent
Coating Z-1	Coating Z-0 + 1.49% nano-ZrO_2 concentrate (1% nano-ZrO_2)
Coating Z-3	Coating Z-0 + 4.48% nano-ZrO_2 concentrate (3% nano-ZrO_2)
Coating Z-5	Coating Z-0 + 7.46% nano-ZrO_2 concentrate (5% nano-ZrO_2)

[1] Z represents nano-ZrO_2. The number shows the wt % of ZrO_2 nanoparticles embedded in the phenolic-epoxy coating.

2.4. Particle Size Analysis of Nano-ZrO_2 Concentrate

Particle sizes were measured using the dynamic light scattering (DLS) technique with the Malvern Zetasizer (Nano ZS). Before the experiment, a small amount of nano-ZrO_2 concentrate was dropped into solvent PMA and ultrasonic shaken for 20 min to produce a concentration of 0.5×10^{-6}. The measurement of particle sizes was performed at room temperature with three repetitions.

2.5. Surface Properties

The surface and cross section panels were cut out of the coated plates before and after the static immersion test. In the case of cross-section, it was embedded in bakelite using an XQ-2B mounting press in order to grind with SiC paper up to 2000 grit, and then it was polished. The surface and cross section morphologies of samples were analyzed by scanning electron microscopy (SEM, XL30-FEG-ESEM, Philips, Amsterdam, Holland) at 20 kV equipped with an energy dispersive spectrometer (EDS) to evaluate element distribution, and a gold film was sprayed atop the surface of samples to make it electrically conductive. The surface morphologies of coatings were characterized by atomic force microscopy (PicoSPM II AFM), by Molecular Imaging Corp. (Bruker Corporation, Saarbrucken, Germany), with a scanning area of 5 μm × 5 μm.

X-ray photoelectron spectroscopy (XPS, Thermo, Waltham, MA, USA) analysis was performed with an ESCALAB250 spectrometer to study the carbon-to-oxygen (C/O) variation in polymers before and after acid immersion, using AlKα excitation radiation (hv = 1486.6 eV). The XPS plot size was 500 μm, and the constant pass energy was 50.0 eV. The XPS depth profile was carried out using Ar^+ ions. The sputtering rate and area were 0.2 nm/s and 2 × 2 mm, respectively. At the same time, the atomic percentages of elements were calculated automatically with a testing instrument. The data was fitted with XPSPEAK4.1. In addition, coatings before immersion were almost the same, and only the Z-0 coating needed to be tested.

2.6. Electrochemical Studies

The electrochemical properties of the coatings were investigated using an electrochemical workstation (PAR273A, Princeton Instruments, Princeton, NJ, USA). Measurements were carried out in a three-electrode cell with mixed acid solution (including 3 wt % H_2SO_4, 1 wt % HCl, 0.5 wt % HNO_3, and 0.2 wt % HF) as an electrolyte. The three-electrode cell included a saturated calomel reference electrode (SCE) filled with saturated KCl solution which served as a reference electrode (RE), a platinum auxiliary electrode with an exposure surface of 13 mm × 13 mm as a counter electrode (CE), and the sample with an exposure surface of 12.56 cm^2 as working electrode (WC). Prior to the electrochemical measurements, the panels were kept in the solution for 30 min in order to stabilize the free corrosion potential.

The electrochemical impedance spectroscopy (EIS) measurements were performed at open circuit potential in an applied frequency range from 100 to 10 mHz, and a sinusoidal perturbation signal with 20 mV amplitude was used. The obtained data were interpreted on the basis of equivalent electrical analogs using ZsimpWin to obtain the fitting parameters.

3. Results and Discussion

3.1. Characterization of Nano-ZrO_2 Concentrates

The size distribution, TEM micrographs, and chemical element mapping of nano-ZrO_2 concentrates are shown in Figure 1. The content of particles less than 100 nm in diameter reached 63.09%, with an average diameter of 74.5 nm (Figure 1a). The TEM observations showed that nano-ZrO_2 particles had a good dispersion state with dimensions of 10–50 nm, and the nano-ZrO_2 powder appeared to be gray and flat (Figure 1b). The EDS analysis and chemical element mapping showed the presence of elements like oxygen (68.07 at %), and Zirconium (31.93 at %) (Figure 1c), which provides direct evidence for the existence of nano-ZrO_2.

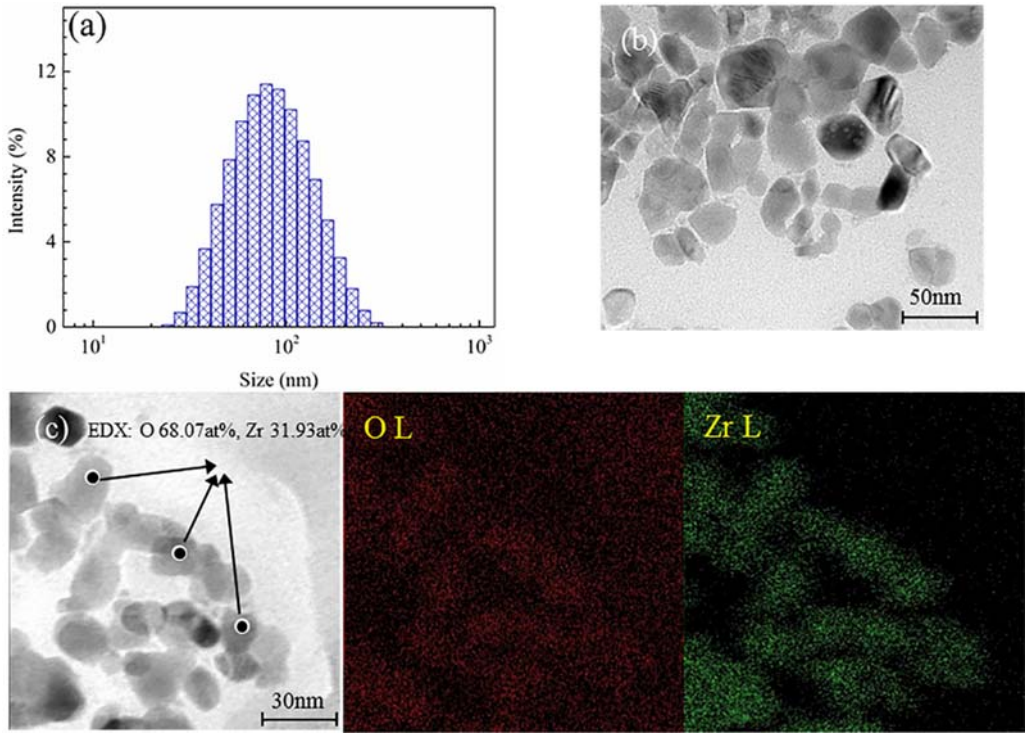

Figure 1. Size distribution (**a**), TEM micrograph (**b**), and chemical element mapping (**c**) of nano-ZrO_2 concentrates.

3.2. Acid Immersion Test and Corrosion Morphologies

Typical SEM micrographs for different nano-ZrO_2-modified coatings before immersion are displayed in Figure 2, along with the EDS analysis in coating Z-5. Pinholes were observed on the surface of the Z-0, Z-1, and Z-5 coatings (Figure 2a,b,d), except for the Z-3 coating (Figure 2c). The aggregation of nano-ZrO_2 appeared on the surface of the Z-5 coating, which implies that the amount of aggregates increased with the nanoparticle content [17]. This was confirmed by the EDS analysis (Figure 2e), which showed the presence of elements like carbon (62.80 at %), zirconium (24.48 at %) and oxygen (12.73 at %).

SEM images of different nano-ZrO_2-modified coatings after 192 h of acid immersion are shown in Figure 3. Various quantities and volumes of pinholes and cracks emerged on the surface of the coatings, which verifies that various levels of degradation occur. Pinholes uniformly distributed on the surface of the Z-0 and Z-1 coatings (Figure 3a,b). Furthermore, pinholes propagated to form cracks on the Z-0 coating. Since 1% nano-ZrO_2 helps to inhibit the initiation and propagation of cracks, no obvious cracks appeared on the Z-1 coating, which demonstrates that the surface of coating Z-1 has better barrier properties than the Z-0 coating. It is necessary to emphasize that the degradation of the Z-3 coating mainly occurred on particular areas of existing fillers, whilst small pinholes formed, and their quantity and volume were much smaller than other coatings at high magnification (Figure 3c). Three percent nano-ZrO_2 dispersed uniformly in the Z-3 coating and generated a network nanostructure, which may be responsible for the improvement in corrosion resistance of the Z-3 coating. By contrast, the deterioration of Z-5 coating was most apparent. Non-uniform corrosion and the largest quantity and volume of pinholes were shown (Figure 3d), arising from the aggregation of excessive nanoparticles. Therefore, the surface of the Z-3 coating has the best barrier properties.

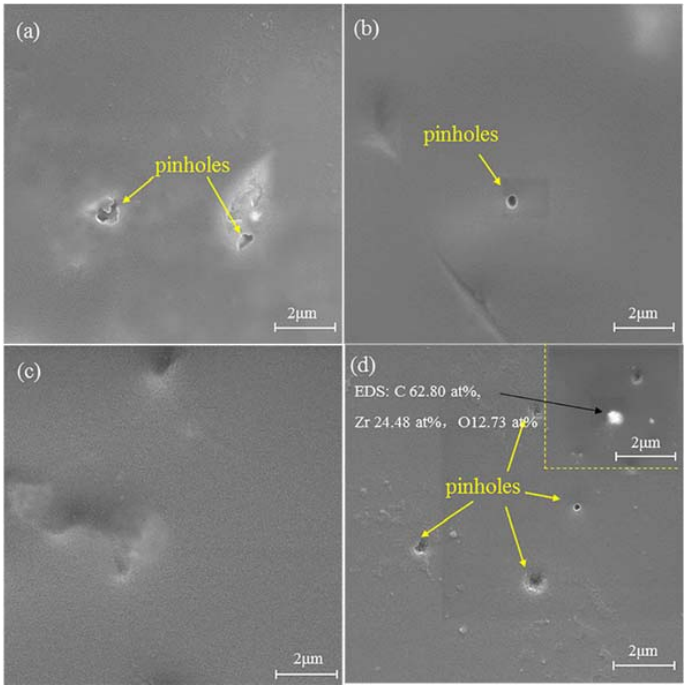

Figure 2. SEM images of different nano-ZrO_2-modified coatings before acid immersion: Z-0 coating (**a**), Z-1 coating (**b**), Z-3 coating (**c**), and Z-5 coating (**d**).

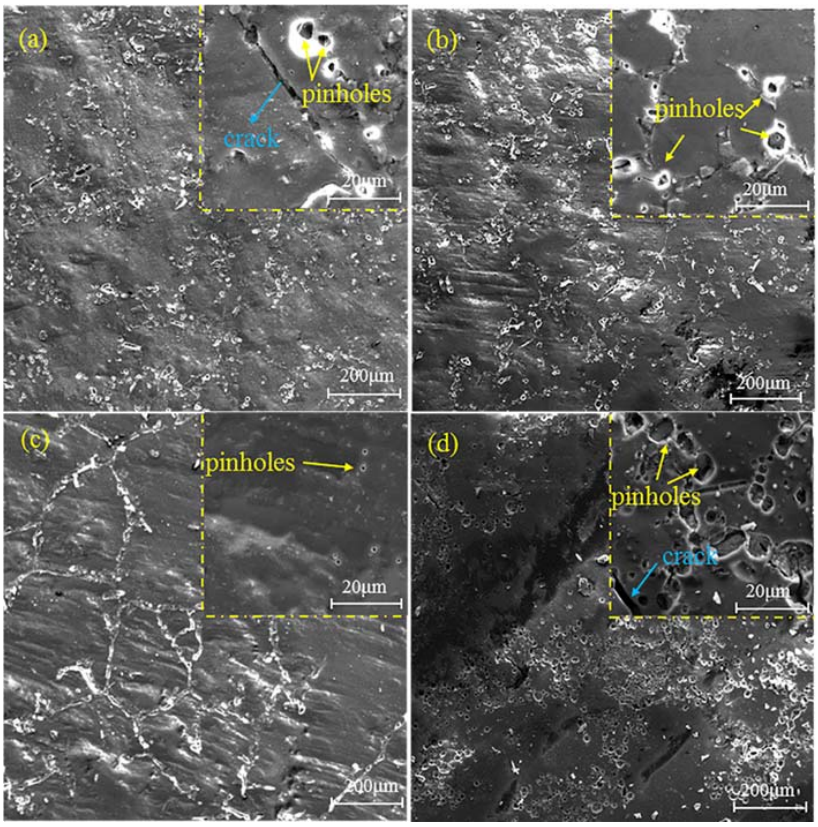

Figure 3. SEM images of different nano-ZrO_2-modified coatings after 192 h of acid immersion: Z-0 coating (**a**), Z-1 coating (**b**), Z-3 coating (**c**), and Z-5 coating (**d**).

Figure 4 exhibits the cross section morphology and elemental mapping for different nano-ZrO_2-modified coatings after 192 h of acid immersion. The cross section morphology showed that obvious cracks appeared at the interface between the substrate and coatings for the Z-0, Z-1 and Z-5 coatings, especially for the Z-5 coating, while the Z-3 coating remained unchanged.

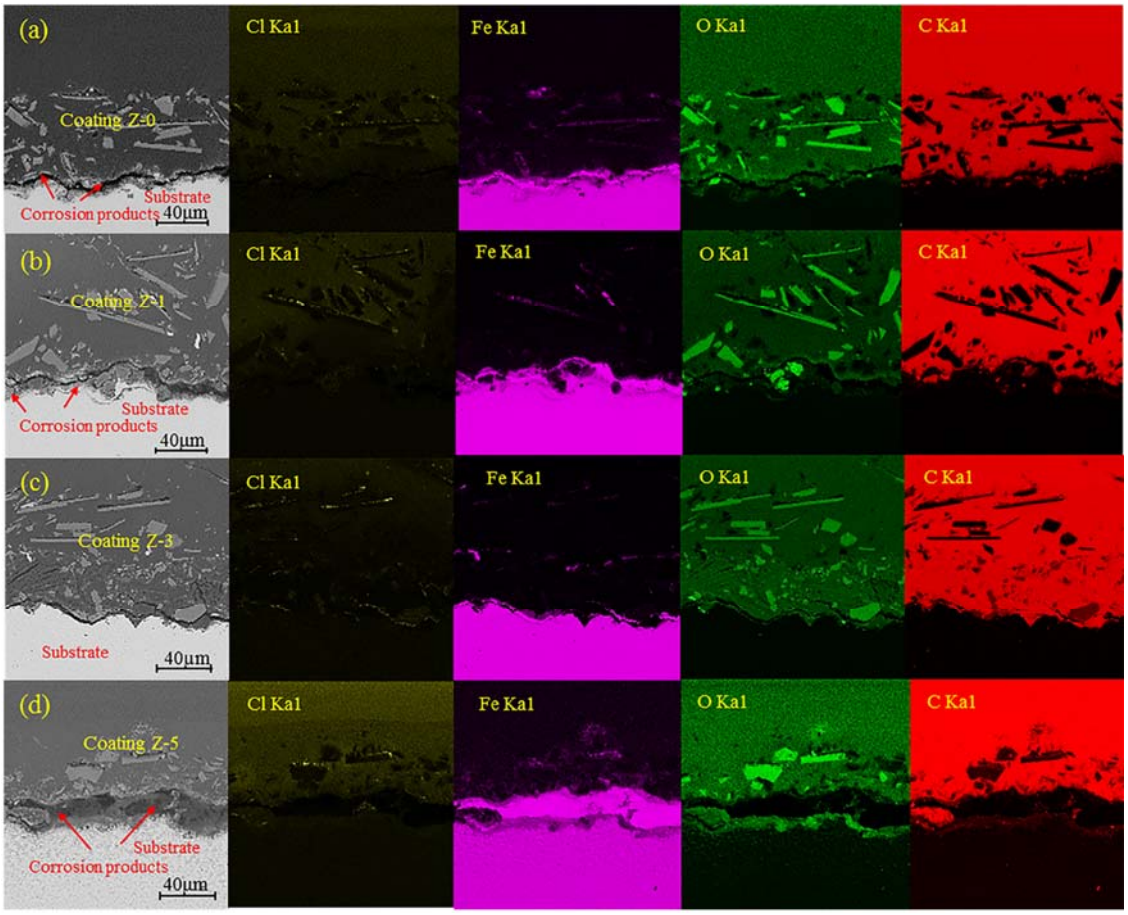

Figure 4. The cross section morphology and chemical element mapping of different nano-ZrO_2-modified coatings after 192 h of acid immersion: Z-0 coating (**a**), Z-1 coating (**b**), Z-3 coating (**c**), and Z-5 coating (**d**).

The elemental mapping revealed that C and O are the major constituents of coatings, and minor amounts of Cl and Fe are also found, which may be introduced from substrates and electrolytes. The big white patches in the oxygen map are glass flakes, and consist of SiO_2, CaO, and Na_2CO_3, corresponding to the low carbon content in carbon map. After 192 h of immersion, corrosive medium went through the coating and reached the metal/coating interface, resulting in the corrosion of substrates. Many iron oxides and hydroxides were generated above the metal substrate, whilst iron ion diffused into the coating via diffusion paths. The concentration of O tended to increase slightly at the metal/coating interface during the immersion period, with the following order: Z-5 coating > Z-0 coating > Z-1 coating > Z-3 coating, corresponding to the distribution sequence of Fe in the coatings. Based on the elemental distributions of O and Fe, different contents of rust formed at the metal–coating interface for these coatings, which revealed that 3% nano-ZrO_2 effectively prevents the permeation of corrosive medium and reduces the generation of rust, whereas 5% nano-ZrO_2 promotes the degradation of coatings.

The same diffusion property was observed for Cl and C. The behavior of Cl^- may be attributed to its penetration through pinholes [18], which implies that the Z-3 coating possesses remarkable Cl^- penetration resistance. Due to the phenomenon of C penetration, degradation of the coatings

occurred in the mixed acid, which provided diffusion paths for carbonaceous species dissociated from coatings, and caused C to accumulate at the metal/coating interface. The distributions of Cl and C also demonstrated that the coatings had suffered various levels of degradation, in the order of 5%, 0, 1%, and 3% nano-ZrO_2 contents.

Internal voids inevitably exist in the coatings, owing to the volatilization of dissolvent and other reasons which provide diffusion paths for small corrosive molecules, such as H^+, Cl^-, and O_2. The diffusion of these corrosive molecules promotes the failure of coatings. The presence of H^+ evidently accelerates the self-degradation rate of coatings [19], and Cl^- reaches the interior of coating through these micro-voids, because of its strong penetration ability. Meanwhile, complete coatings cannot block the attack of acid medium, which causes the nucleation of new micro-voids. Micro-voids grow up with the immersion time, and larger corrosive molecules go through and accumulate at the metal–coating interface, such as carbonaceous species. The nano-ZrO_2 addition changes the size and amount of internal voids, which has an impact on the corrosion resistance of coatings. The specific effect of nano-ZrO_2 content on the variation of voids for coatings is discussed in the following EIS sections.

AFM images of different nano-ZrO_2-modified coatings after 192 h immersion are shown in Figure 5, as well as the average roughness (R_a) and root mean square (*RMS*), as deduced from the AFM analysis, are presented in Table 2. Small hill-shaped degradation products were observed on the surface of the Z-0coating, and the main component was carbohydrates. Some flaky degradation products completely separated from the binder due to embrittlement and poor adhesion [20], leading to the highest R_a (24.58 nm) and *RMS* (73.60 nm) values for the Z-0 coating. With the addition of 1% nano-ZrO_2, the surface topography for the Z-1 coating changed and refined. Only smaller, regular micro-bulges like hills appeared on the surface, which resulted in a lower R_a value of 12.79 nm and *RMS* value of 27.44 nm. With an increase in nano-ZrO_2 content, the smallest micro-bulges were observed on the surface of the Z-3 coating, and the R_a and *RMS* values reduced to 5.94 nm and 16.10 nm, respectively, in spite of existing amorphous bulges and micro-holes. However, when the nano-ZrO_2 content reached 5%, the corrosion resistance of the Z-5 coating declined significantly. Patches of micro-bulges became larger, and flaky degradation products were faintly visible, which led to an increase in the R_a (20.42 nm) and *RMS* values (52.03 nm). In addition, the R_a value of the Z-5 coating was lower than that of the Z-0 coating, which resulted from the severe inhomogeneous corrosion of the Z-5 coating and a limited scanning area for AFM. In short, the addition of 3% nano-ZrO_2 minimized the average roughness and root mean square values, which effectively improved the corrosion resistance of the coating.

Table 2. R_a and root mean square (*RMS*) values of different nano-ZrO_2-modified coatings after 192 h of acid immersion, as deduced from AFM analysis.

Samples	R_a (nm)	*RMS* (nm)
Z-0 Coating	24.58	73.60
Z-1 Coating	12.79	27.44
Z-3 Coating	5.94	16.10
Z-5 Coating	20.42	52.03

Due to high surface sensitivity and chemical specificity, XPS was used to better understand the exposure-induced bond failure and component variation in the organic coatings during the corrosion test [7]. Figure 6 shows the XPS spectra (C1s and O1s) and atomic ratio (C/O) of the Z-0, Z-1, Z-3, and Z-5 coatings before and after acid immersion, and the corresponding atomic compositions are given in Table 3. The C1s and O1s XPS peaks of four coatings were at about 281.4 eV and 528.6 eV, respectively. The XPS intensity data were converted into units of at %, and the images provide detailed elemental components. The C1s and O1s spectra were peak-fitted to deduce the concentrations of carbon and oxygen.

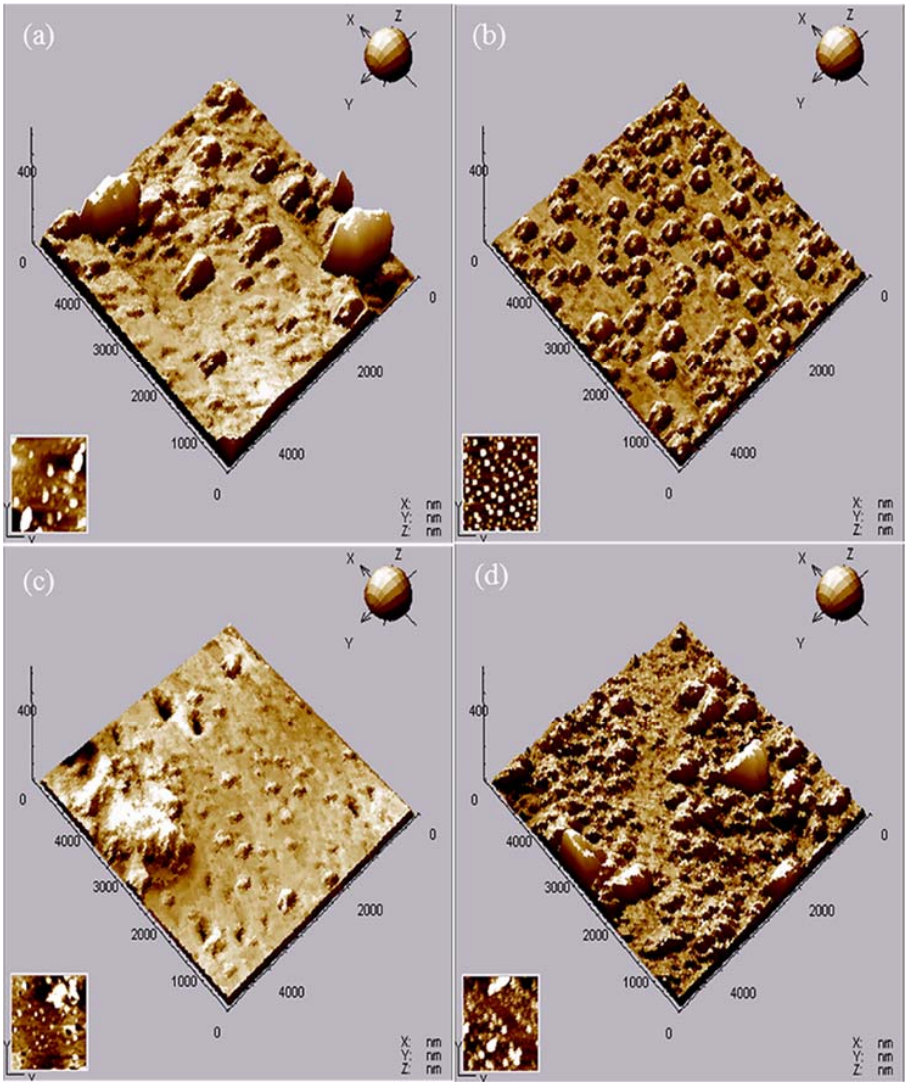

Figure 5. AFM images of different nano-ZrO_2-modified coatings after 192 h acid immersion: Z-0 coating (**a**), Z-1 coating (**b**), Z-3 coating (**c**), and Z-5 coating (**d**).

Table 3. Atomic compositions (at %) derived from XPS survey spectra for the Z-0, Z-1, Z-3 and Z-5 coatings before and after acid immersion.

	Samples	Element	At %
Before immersion	Z-0, Z-1, Z-3 and Z-5 Coatings	C1s	79.86
		O1s	17.01
		N1s	1.8
After immersion	Z-0 Coating	C1s	77.82
		O1s	20.47
		N1s	1.71
	Z-1 Coating	C1s	80.37
		O1s	18.46
		N1s	1.16
	Z-3 Coating	C1s	80.77
		O1s	17.31
		N1s	1.93
	Z-5 Coating	C1s	76.99
		O1s	19.81
		N1s	3.21

Due to strong oxidation and ion permeation at high temperatures, mixed acid initiates the scission of molecular chain and degradation of the polymer network [7]. The general trend is a decrease in C content, which is related to the migration of carbonaceous species from the surface. The amount of O on the surface generally increases, due to the superficial oxidation and water adsorption upon storage [21]. The contents of C, O, and N elements of the Z-0 coating before acid immersion were 79.86%, 17.01%, and 1.80%, respectively, while after acid immersion, these changed to 77.82%, 20.47%, and 1.71%. This is a consequence of the migration of carbonaceous species and superficial oxidation. In addition, the C/O ratio of the Z-0 coating decreased from 4.69 (before acid immersion) to 3.89 (after acid immersion), suggesting that the stability and component of the Z-0 coating was strongly damaged, due to the chemical decomposition.

With the addition of 1% nano-ZrO_2, the C and O contents after acid immersion for the Z-1 coating increase to 80.37 at % and 18.46 at%, respectively. The C/O value decreases from 4.69 (before acid immersion) to 4.30 (after acid immersion), which is obviously larger than that of the Z-0 coating, demonstrating that 1% nano-ZrO_2 can inhibit the migration of carbonaceous species and superficial oxidation to a certain degree. With an increase in the nano-ZrO_2 content, the concentrations of C and O after acid immersion for the Z-3 coating increased to 80.77 at %, and 17.31 at %, respectively. The reduction degree of the C/O value of the Z-3 coating was the smallest, decreasing from 4.69 (before acid immersion) to 4.55 (after acid immersion). The high C/O ratio was directly connected with good anti-oxidation and corrosion resistance, implying that 3% nano-ZrO_2 provided the physical barrier for corrosive media to permeate, and suppressed the migration of carbonaceous species and superficial oxidation. When the nano-ZrO_2 content reached 5%, the C content after acid immersion of the Z-5 coating reduced significantly, while the O content increased greatly. Correspondingly, the C/O value after acid immersion (3.88) decreased to the minimum, and it was even lower than that of the Z-0 coating. Excessive nano-ZrO_2 led to a decline of the anticorrosion property of coatings, and promoted the migration of carbonaceous species and superficial oxidation. In conclusion, XPS analyses showed that Z-3 coating had the best anticorrosion property.

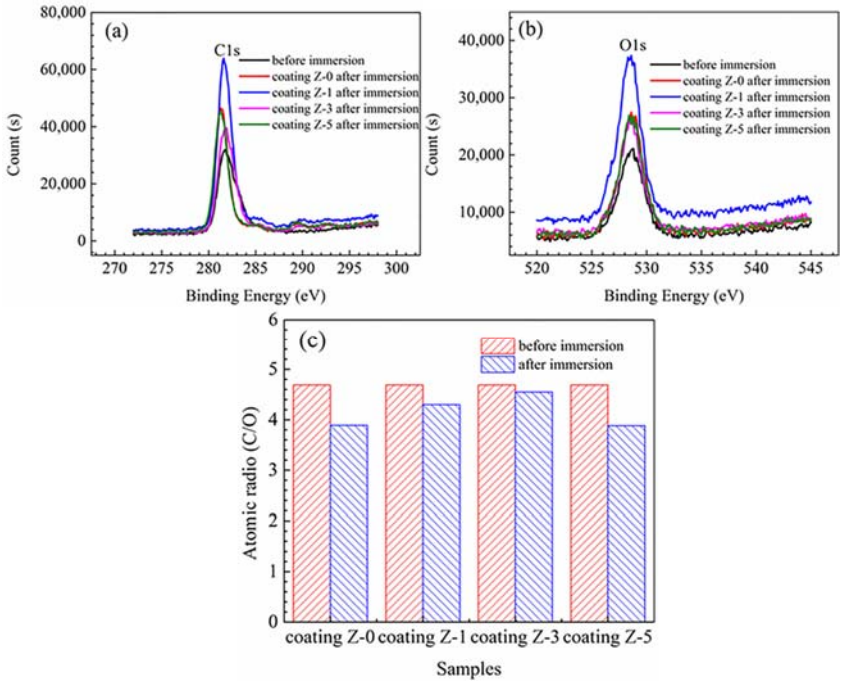

Figure 6. XPS spectra (C1s (**a**), O1s (**b**)) and atomic radio (C/O) (**c**) of the Z-0, Z-1, Z-3, and Z-5 coatings before and after acid immersion.

3.3. Electrochemically-Evaluated Corrosion Response

Figure 7 shows the OCP variation in the nano-ZrO_2-modified coatings with the immersion time. The initial OCP of the bare substrate was –485 mV vs. SCE, and this shifted towards a more cathodic region with time. After 24 h of immersion, it became a steady-state value (–601 mV vs. SCE). In the beginning, the OCP values of the Z-1 coating, the Z-0 coating, the Z-5 coating, and the Z-3 coating were more positive than that of the bare substrate, and increased by 133 mV, 149 mV, 157 mV, and 184 mV, respectively, which clearly indicates the high corrosion resistance provided by these coatings [22]. With a prolonged immersion time, the OCPs of all the coatings presented a similar tendency towards lower values, arising from the diffusion of electrolytes and corrosive ions through coating defects and pinholes [23]. After 120 h of immersion, the potential difference between coatings and bare substrate decreased to 54 mV, 81 mV, 85 mV, and 101 mV for the Z-5 coating, Z-0 coating, Z-1 coating, and Z-3 coating, respectively, indicating that the protection performance of coatings deteriorates continuously with immersion time [24]. After 192 h of immersion, the OCPs of all the coatings reduced towards a negative potential to be lower than bare substrate, except for the Z-3 coating. This is probably due to the heterogeneous reactions arising from the formation of large diffusion paths within coatings [25,26] or the occurrence of some surface phenomena, such as the diffusion of chloride ions through the coating [27]. Consequently, the Z-3 coating exhibited the highest OCP value during the immersion, which demonstrates that the addition of 3% nano-ZrO_2 effectively improves the anticorrosion property of coatings.

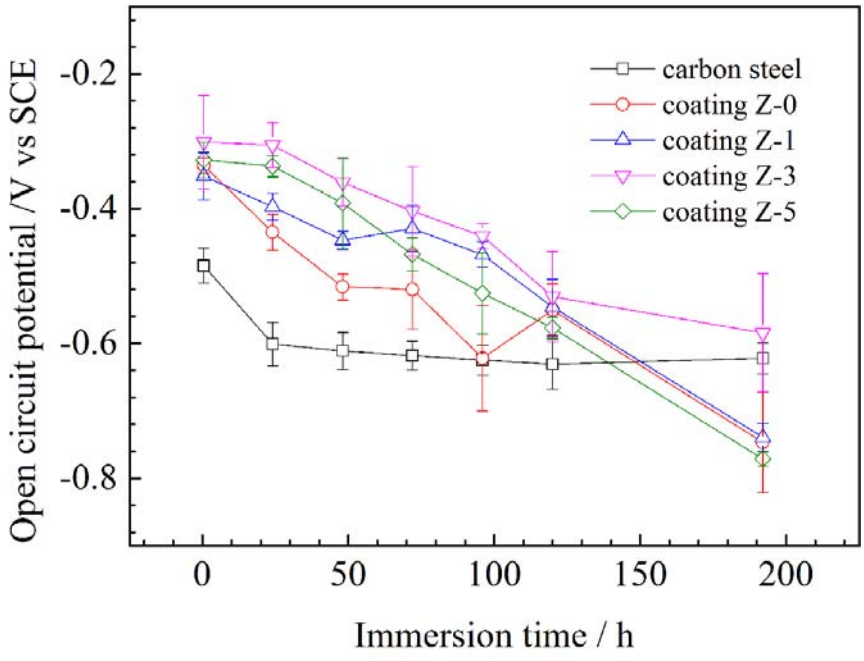

Figure 7. OCP variations of different nano-ZrO_2-modified coatings in mixed acid solution at 60 °C.

The typical EIS diagrams measured for various nano-ZrO_2-modified coatings after 30 min, 24 h, 120 h, and 192 h immersion are presented in Figure 8. The equivalent electrical circuits shown in Figure 9 were used to fit the measured data, and the fitted lines are presented along with the measured data points. The equivalent electrical circuits are addressed in detail in the next section.

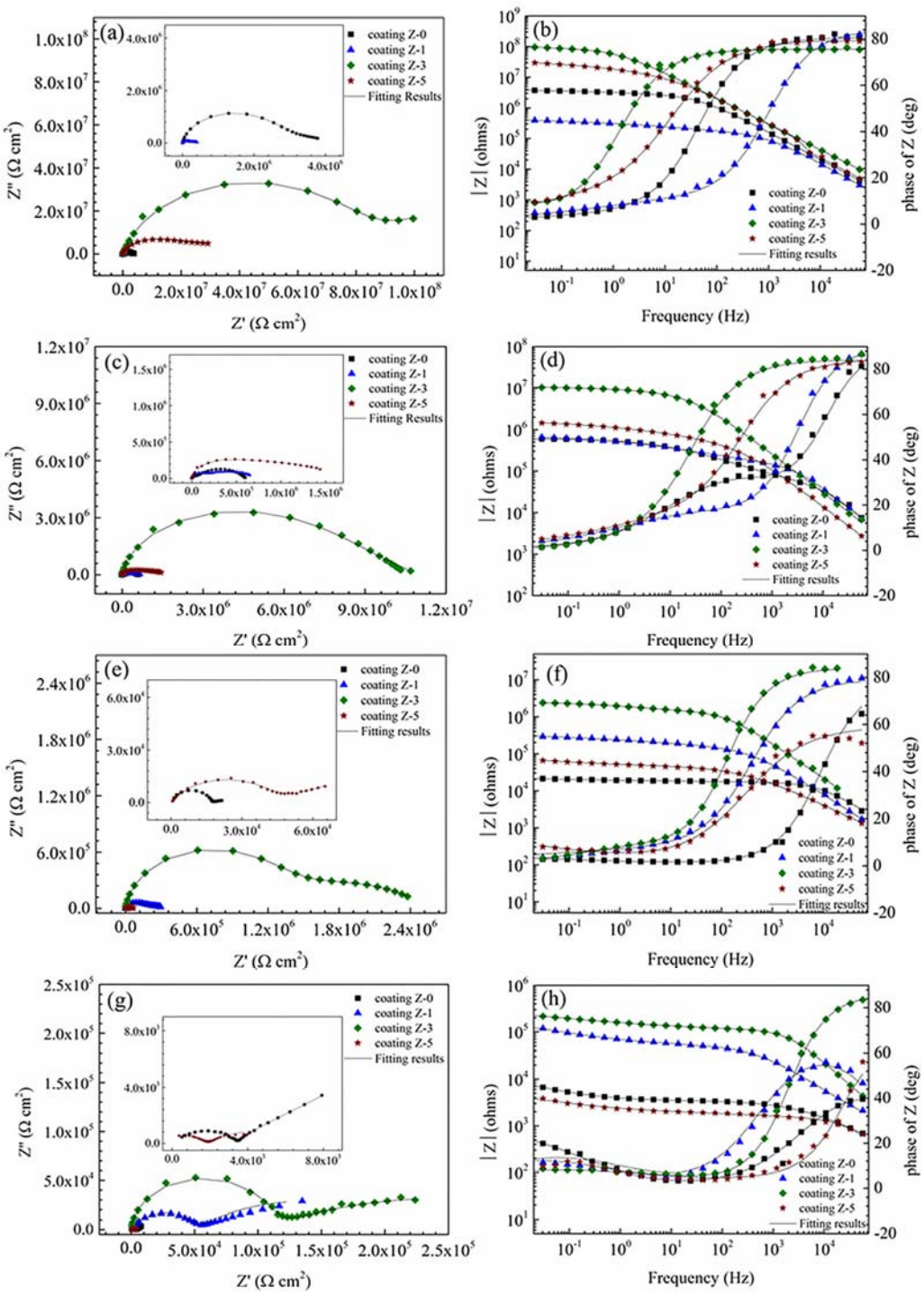

Figure 8. Typical Nyquist and Bode plots for nano-ZrO_2-modified coatings after different acid immersion times at 60 °C: 30 min (**a**,**b**), 24 h (**c**,**d**), 120 h (**e**,**f**), and 192 h (**g**,**h**).

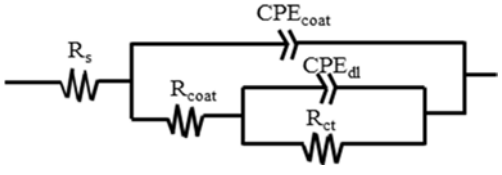

Figure 9. Equivalent circuit model for samples: $R_s(Q_{coat}(R_{coat}(Q_{dl}R_{ct})))$.

The EIS diagrams for all of the coatings showed two time constants. The high frequency time constant shows the barrier properties of the coating, and the low frequency time constant corresponds to the polarization resistance of steel surface beneath the coating layer [23,27–30]. A shift of phase angle to higher frequency region demonstrates that an increased area of coated substrate is exposed to the corrosive environment [31]. The Z-3 coating showed a high frequency phase angle in the lower frequency region, indicating its superior coating barrier property. The low frequency impedance modulus, $|Z|_{LF}$ (e.g., $|Z|_{0.01Hz}$) is commonly used to roughly estimate the coating resistance [32]. The $|Z|_{LF}$ of the Z-0 coating presented a clear tendency to decrease with the immersion time. After 24 h of immersion, $|Z|_{LF}$ decreased below 10^6 Ω·cm^2, and a horizontal line section appeared at the middle frequency, which is characteristic of the delamination of a coating [2,33]. After 192 h of immersion, the $|Z|_{LF}$ was even lower than 10^4 Ω·cm^2. The $|Z|_{LF}$ of the Z-1 coating increased firstly and then decreased with the immersion time. Though it was lower in the beginning, the $|Z|_{LF}$ was much higher than that of the Z-0 coating after 192 h of immersion, which testifies that 1% nano-ZrO_2 has a limited improvement on the anticorrosion property. The $|Z|_{LF}$ of the Z-3 and Z-5 coatings kept decreasing with the immersion time. The $|Z|_{LF}$ of the Z-3 coating was about 10^8 Ω·cm^2 in the beginning, and it remained the largest among all the coatings, even after 192 h of immersion, which demonstrates that 3% nano-ZrO_2 efficiently improves the coating resistance. The $|Z|_{LF}$ of coating Z-5 decreased rapidly from 10^7 Ω·cm^2, to a value lower than that of coating Z-0 after 192 h of immersion, which means that an excessive concentration of nano-ZrO_2 has a negative effect on the anticorrosion property of a coating. Therefore, when the nano-ZrO_2 content reached 3%, the anticorrosion property of coatings performed best, and then decreased with an increase in the nano-ZrO_2 content.

The EIS data were fitted by the equivalent circuit $R_s(Q_{coat}(R_{coat}(Q_{dl}R_{ct})))$ shown in Figure 9 using ZsimpWin [34]. In these circuits, R_s is the solution resistance, Q_{coat} is the constant phase element (CPE) of a coating, R_{coat} is the resistance of the electrolyte in the coating pores, Q_{dl} is the CPE of the electrical double layer, and R_{ct} is the charge transfer resistance.

The CPE was substituted for pure capacitance, due to surface heterogeneities, deviation from capacitive behavior, and dispersion effects [35]. The impedance of CPE can be written as:

$$Z_{CPE} = \frac{1}{Q(j\omega)^{\alpha}}, \quad (1)$$

where Q is the CPE constant, $j = \sqrt{-1}$, ω is the angular frequency (rad/s), and α is a CPE exponent associated with the surface heterogeneity or roughness [36]. When $\alpha < 1$, the CPE parameter (Q) cannot represent the capacitance, and the effective capacitance (*Ceff*) associated with the CPE can therefore be expressed as [37]:

$$Ceff_{coat} = Q^{\frac{1}{\alpha}} \left(\frac{R_s \cdot R_{coat}}{R_s + R_{coat}} \right)^{\frac{1-\alpha}{\alpha}}. \quad (2)$$

Table 4 presents the electrical element parameters obtained from fitting the measured EIS data in Figure 8. The change in electrical element parameters reflects the change in the electrochemical properties of the coated system [38]. It is generally accepted that the increase in $Ceff_{coat}$ with time is related to the water uptake [39] and the dielectric constant [40] of the coating; R_{coat} is attributed to the electrical resistance to ionic transfer through the coating pores, which reflects the porosity of coatings and the anti-penetrating ability to the electrolyte solution [31,41]; R_{ct} is used to specify the delamination of the top coat and the onset of substrate corrosion [42], which is inversely proportional to the surface area of the sample [43]. In general, a good coating system is characterized by high resistances (R_{coat} and R_{ct}), lower capacitances ($Ceff_{coat}$) [44].

Table 4. Fitting results of EIS for the Z-0, Z-1, Z-3, and Z-5 coatings after different acid immersion times.

Sample	Immersion Time/h	R_s/Ω·cm^2	Q_{coat}/s^n ·Ω^{-1}·cm^{-2}	α_{coat}	$Ceff_{coat}$/F·cm^{-2}	R_{coat}/Ω·cm^{-2}	Q_{dl}/s^n· Ω^{-1}·cm^{-2}	α_{dl}	R_{ct}/Ω·cm^2	*Chsq*
Z-0 Coating	30 min	0.36	2.44×10^{-9}	0.896	2.16×10^{-10}	1.81×10^{6}	2.02×10^{-7}	0.2517	2.54×10^{6}	1.30×10^{-3}
	24 h	0.36	3.41×10^{-10}	1	3.41×10^{-10}	4.60×10^{4}	1.67×10^{-7}	0.5321	5.63×10^{5}	2.21×10^{-3}
	120 h	393	2.88×10^{-9}	0.9113	7.59×10^{-10}	1.48×10^{4}	1.99×10^{-4}	0.1117	2.53×10^{5}	3.59×10^{-4}
	192 h	138	4.84×10^{-7}	0.6298	1.66×10^{-9}	3.26×10^{3}	5.58×10^{-4}	0.4868	2.84×10^{4}	1.94×10^{-4}
Z-1 Coating	30 min	0.36	2.10×10^{-9}	0.9337	4.73×10^{-10}	9.51×10^{4}	1.17×10^{-6}	0.296	3.70×10^{5}	2.12×10^{-3}
	24 h	0.37	3.88×10^{-10}	1	3.88×10^{-10}	1.11×10^{5}	4.76×10^{-7}	0.3895	6.08×10^{5}	1.16×10^{-3}
	120 h	0.36	7.46×10^{-9}	0.8793	4.97×10^{-10}	6.89×10^{4}	2.24×10^{-6}	0.1965	3.58×10^{5}	9.63×10^{-4}
	192 h	723	4.89×10^{-8}	0.7395	1.32×10^{-9}	5.10×10^{4}	2.47×10^{-5}	0.4372	1.52×10^{5}	3.34×10^{-3}
Z-3 Coating	30 min	0.36	2.16×10^{-9}	0.8403	4.02×10^{-11}	8.26×10^{7}	1.07×10^{-7}	0.4962	1.11×10^{8}	1.68×10^{-3}
	24 h	0.36	1.09×10^{-9}	0.9344	2.37×10^{-10}	2.38×10^{6}	1.76×10^{-8}	0.3601	8.67×10^{6}	2.37×10^{-3}
	120 h	0.36	1.52×10^{-9}	0.9331	3.28×10^{-10}	1.26×10^{6}	3.28×10^{-7}	0.4515	1.31×10^{6}	2.15×10^{-3}
	192 h	0.36	1.11×10^{-9}	0.9572	4.21×10^{-10}	1.04×10^{5}	8.61×10^{-6}	0.2803	2.80×10^{5}	3.97×10^{-4}
Z-5 Coating	30 min	0.36	2.47×10^{-9}	0.8815	1.50×10^{-10}	3.21×10^{6}	2.67×10^{-8}	0.2855	4.09×10^{7}	2.55×10^{-3}
	24 h	0.36	2.34×10^{-9}	0.9338	5.31×10^{-10}	2.01×10^{5}	2.61×10^{-7}	0.3371	1.49×10^{6}	2.29×10^{-3}
	120 h	228	1.19×10^{-7}	0.6911	1.08×10^{-9}	4.31×10^{4}	4.41×10^{-5}	0.3982	4.53×10^{4}	4.51×10^{-4}
	192 h	67.3	2.35×10^{-8}	0.8619	2.74×10^{-9}	1.41×10^{3}	5.10×10^{-4}	0.2736	5.76×10^{3}	4.13×10^{-4}

The plots in Figure 10a–c clearly show the variation trends of $Ceff_{coat}$, R_{coat} and R_{ct} for the coatings versus the immersion time. The $Ceff_{coat}$ of all of the coatings was very low (less than 10^{-8}), indicating the insulating nature of the coatings [28]. At the beginning of the test, all of the coatings showed high resistances (R_{coat} and R_{ct}) and low $Ceff_{coat}$, except for the Z-1 coating. The $Ceff_{coat}$ value of the coatings increased in the following order: Z-3 coating, Z-5 coating, Z-0 coating, and Z-1 coating. This shows that the water resistance of coatings does not increase with the nano-ZrO_2 content. For the 1% nano-ZrO_2 content, the nano-ZrO_2 particle tended to sink into the coating due to its high density during the curing process, and larger micro-channels emerged on the top of the coating in the initial stage, which led to the Z-1 coating having the lowest resistances (R_{coat} and R_{ct}) and highest $Ceff_{coat}$. When the nano-ZrO_2 content increased to 3%, nano-ZrO_2 particles were able to uniformly distribute in the coating and the hole sealing effect had an absolute advantage over agglomeration, which effectively improved the resistances (R_{coat} and R_{ct}) and led to a decline in $Ceff_{coat}$ in the Z-3 coating. As the nano-ZrO_2 content reached 5%, the dominant status of the hole-sealing effect in the nano-particles was challenged by aggregation, which led to a decline in resistance (R_{coat} and R_{ct}) and an increase in $Ceff_{coat}$ of the Z-5 coating to some degree.

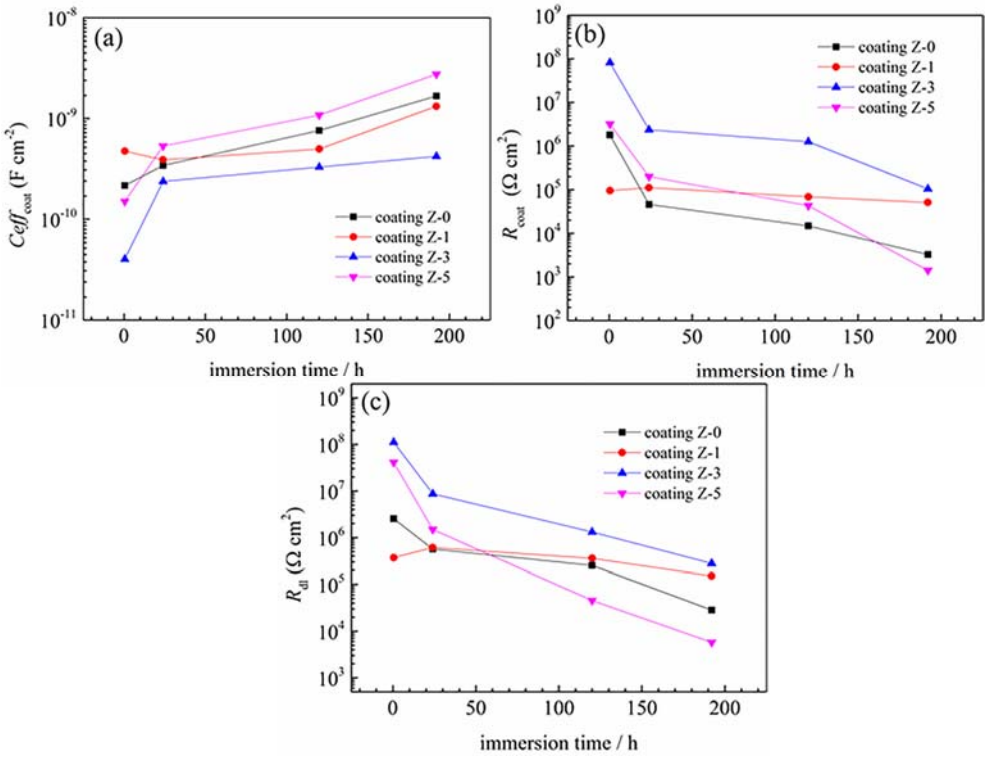

Figure 10. Variations of $Ceff_{coat}$, R_{coat}, and R_{ct} with immersion time (values from Table 4).

With a prolonged immersion time, there was a prominent decrease in the resistances (R_{coat} and R_{ct}) and an increase in $Ceff_{coat}$ for most coatings, due to the development of pathways. In particular, the $Ceff_{coat}$ of the Z-1 coating decreased firstly and then increased with an increased immersion time, while the resistances (R_{coat} and R_{ct}) increased and then decreased. This implies that 1% nano-ZrO_2 takes effect when the corrosive medium permeates into the lower part of the Z-1 coating. Additionally, the hole-sealing effect of insoluble corrosion products [45] should not be neglected, as confirmed in the shift of the R_{coat} value.

After 192 h of immersion, the significant decrease in the resistance and increase in $Ceff_{coat}$ indicated that the corrosion process had occurred. With an increase in the nano-ZrO_2 content, the corrosion process was inhibited firstly and then promoted, and the inhibition effect of 3% nano-ZrO_2 was the most significant. The $Ceff_{coat}$, R_{coat} and R_{ct} of the Z-3 coating were 0.25, 31.90 and 9.86 times that of

coating Z-0, respectively, which indicates a markedly enhanced water resistance, lower porosity and larger charge transfer resistance.

To further understand the anticorrosion mechanism of the nano-ZrO_2-modified coatings in mixed acid solution, a schematic interpretation is depicted in Figure 11. As shown in Figure 11a, the Z-0 coating has abundant voids and defects, which provides preferential diffusion paths for corrosive species of Cl^-, H^+, and O_2, etc. When a corrosive medium reaches the metal–coating interface, the following corrosion process for the substrate is proposed:

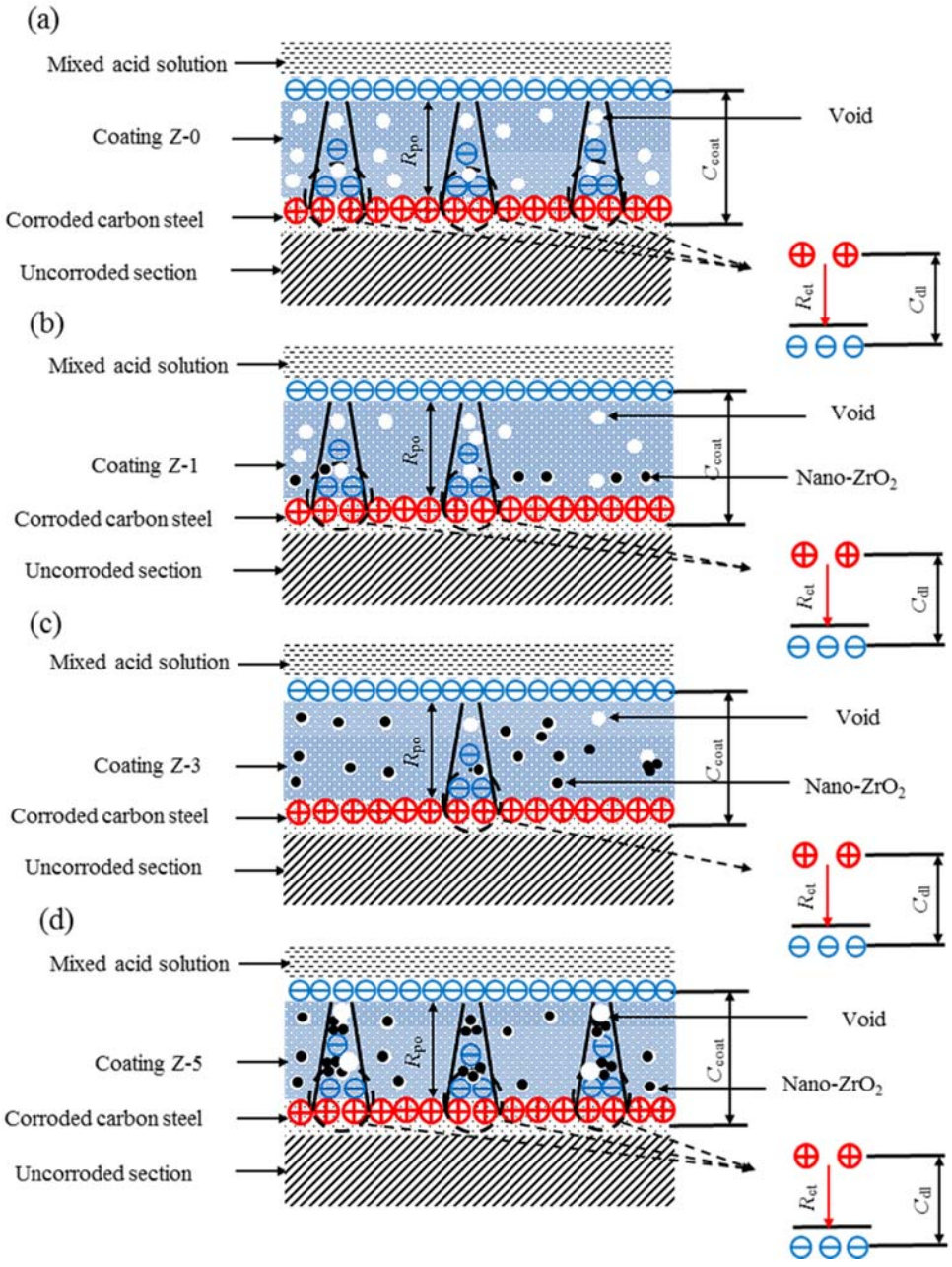

Figure 11. Schematic illustrations of corrosion process for the Z-0 (**a**), Z-1 (**b**), Z-3 (**c**) and Z-5 (**d**) coatings: ⊕: positive charge, ⊖: negative charge.

Anodic reaction:

$$Fe - 2e^- \rightarrow Fe^{2+}. \quad (3)$$

Cathodic reaction:

$$2H^+ + 2e^- \rightarrow H_2. \quad (4)$$

The nano-ZrO_2 addition did not change the reaction mechanism of the substrates. With an increase in the nano-ZrO_2 content, the micro-pore channels gradually sealed, while excessive nano-ZrO_2 caused agglomeration and produced larger micro-pore channels when corrosion occurred. The competition relationship between agglomeration and the hole-sealing effect of nano-particles was obviously visible. The addition of 1% nano-ZrO_2 partially sealed micro-pore channels of the Z-1 coating (Figure 11b), and generated an incomplete nanostructure network, which was responsible for the limited improvement of corrosion resistance. In contrast, the addition of 3% nano-ZrO_2 perfectly balanced the relationship between agglomeration and the sealing of micro-pore channels of nano-particles, and formed a relatively complete nanostructure network, which effectively improved the corrosion resistance of the Z-3 coating (Figure 11c). When the nano-ZrO_2 content reached 5%, the corrosion resistance of the Z-5 coating dramatically reduced. Nano-particles still sealed micro-pore channels, while lots of agglomerations occurred for the Z-5 coating (Figure 11d). Thus, the Z-3 coating showed the best anticorrosion property.

4. Conclusions

The corrosion protection characterizations for nano-ZrO_2-modified coatings were examined in mixed acid solution. Corrosion resistance was enhance for the coatings with 1% and 3% nano-ZrO_2 contents, while it declined for the coating with 5% nano-ZrO_2 content. The 3% nano-ZrO_2 particle modified coating showed the best corrosion protection performance, as evidenced by EIS results. Visual assessments through SEM, AFM and elemental mapping observations were in accordance with the electrochemical results.

One percent nano-ZrO_2, with an incomplete nanostructure network in the coating, showed a limited improvement to the anticorrosion property, and 5% nano-ZrO_2 led to excessive aggregation and declined the adhesion of reinforced nanoparticles, which damaged the corrosion resistance. Three percent nano-ZrO_2 possesses remarkable dispersion properties and a relatively complete nanostructure network in the coating, and was shown to balance the relationship between agglomeration and sealing of the micro-pore channels of nano-particles perfectly, which resulted in a minimum amount of diffusion of Cl, C, O and Fe, the lowest average roughness (5.94 nm), the highest C/O radio (4.55), and the best electrochemical properties (highest resistances and lowest $Ceff_{coat}$).

Author Contributions: Z.W. and W.X. designed the research. W.X. and S.W. performed the mathematical calculations. W.X., Z.W., S.W. and Q.L. discussed and analyzed the data. W.X. wrote the manuscript. Z.W. and E.-H.H. revised the paper.

Funding: This work was supported by the Key Technology of Corrosion Control on Wind Power Equipment Academician Workstation Project (Grant No. 2013B090400023).

Acknowledgments: The authors are grateful to M.C. Yan for the language revision.

Conflicts of Interest: The authors declare no conflict of interest.

References

1. Stanger, R.; Wall, T. Sulphur impacts during pulverised coal combustion in oxy-fuel technology for carbon capture and storage. *Prog. Energy Combust. Sci.* **2011**, *37*, 69–88. [CrossRef]
2. Shi, H.W.; Liu, F.C.; Yang, L.H.; Han, E.H. Characterization of protective performance of epoxy reinforced with nanometer-sized TiO_2 and SiO_2. *Prog. Org. Coat.* **2008**, *62*, 359–368. [CrossRef]
3. Moller, V.B.; Dam-Johansen, K.; Frankaer, S.M.; Kiil, S. Acid-resistant organic coatings for the chemical industry: A review. *J. Coat. Technol. Res.* **2017**, *14*, 279–306. [CrossRef]
4. Shi, X.M.; Nguyen, T.A.; Suo, Z.Y.; Liu, Y.J.; Avci, R. Effect of nanoparticles on the anticorrosion and mechanical properties of epoxy coating. *Surf. Coat. Technol.* **2009**, *204*, 237–245. [CrossRef]

5. Mayavan, S.; Siva, T.; Sathiyanarayanan, S. Graphene ink as a corrosion inhibiting blanket for iron in an aggressive chloride environment. *RSC Adv.* **2013**, *3*, 24868–24871. [CrossRef]
6. Cech, J.; Kretow, B. The effectiveness of toughening technologies on multifunctional epoxy resin systems. *Surf. Coat. Aust.* **2003**, *40*, 19–23.
7. Wang, Z.; Han, E.; Liu, F.; Ke, W. Effect of Different Curing Agents on Cure Reaction and Exposure Resistance of Phenolic-Epoxy Resins in Hot Acid Solutions. *Corrosion* **2010**, *66*. [CrossRef]
8. Sabzi, M.; Mirabedini, S.M.; Zohuriaan-Mehr, J.; Atai, M. Surface modification of TiO_2 nano-particles with silane coupling agent and investigation of its effect on the properties of polyurethane composite coating. *Prog. Org. Coat.* **2009**, *65*, 222–228. [CrossRef]
9. Alexandre, M.; Dubois, P. Polymer-layered silicate nanocomposites: Preparation, properties and uses of a new class of materials. *Mater. Sci. Eng. R Rep.* **2000**, *28*, 1–63. [CrossRef]
10. Chaiko, D.J.; Leyva, A.A. Thermal transitions and barrier properties of olefinic nanocomposites. *Chem. Mater.* **2005**, *17*, 13–19. [CrossRef]
11. Hang, T.T.X.; Truc, T.A.; Nam, T.H.; Oanh, V.K.; Jorcin, J.B.; Pebere, N. Corrosion protection of carbon steel by an epoxy resin containing organically modified clay. *Surf. Coat. Technol.* **2007**, *201*, 7408–7415. [CrossRef]
12. Song, H.-J.; Zhang, Z.-Z. Investigation of the tribological properties of polyfluo wax/polyurethane composite coating filled with nano-SiC or nano-ZrO_2. *Mater. Sci. Eng. A* **2006**, *426*, 59–65. [CrossRef]
13. Behzadnasab, M.; Mirabedini, S.M.; Kabiri, K.; Jamali, S. Corrosion performance of epoxy coatings containing silane treated ZrO_2 nanoparticles on mild steel in 3.5% NaCl solution. *Corros. Sci.* **2011**, *53*, 89–98. [CrossRef]
14. Montesperelli, G.; Gusmano, G.; Rapone, M.; Padeletti, G.; Cusma, A.; Kaciulis, S.; Mezzi, A.; Di Maggio, R. Zirconia primers for corrosion resistant coatings. *Surf. Coat. Technol.* **2007**, *201*, 5822–5828.
15. Ebrahim-Ghajari, M.; Allahkaram, S.R.; Mahdavi, S. Corrosion behaviour of electrodeposited nanocrystalline Co and Co/ZrO_2nanocomposite coatings. *Surf. Eng.* **2014**, *31*, 251–257. [CrossRef]
16. Hu, C.B.; Zheng, Y.S.; Qing, Y.Q.; Wang, F.L.; Mo, C.Y.; Mo, Q. Preparation of Poly(o-toluidine)/Nano Zirconium Dioxide (ZrO_2)/Epoxy Composite Coating and Its Corrosion Resistance. *J. Inorg. Organomet. Polym. Mater.* **2015**, *25*, 583–592. [CrossRef]
17. Zhou, C.L.; Lu, X.; Xin, Z.; Liu, J.; Zhang, Y.F. Polybenzoxazine/SiO_2 nanocomposite coatings for corrosion protection of mild steel. *Corros. Sci.* **2014**, *80*, 269–275. [CrossRef]
18. Sababi, M.; Pan, J.S.; Augustsson, P.E.; Sundell, P.E.; Claesson, P.M. Influence of polyaniline and ceria nanoparticle additives on corrosion protection of a UV-cure coating on carbon steel. *Corros. Sci.* **2014**, *84*, 189–197. [CrossRef]
19. Liang, Y.; Wang, M.D.; Wang, C.; Feng, J.; Li, J.S.; Wang, L.J.; Fu, J.J. Facile Synthesis of Smart Nanocontainers as Key Components for Construction of Self-Healing Coating with Superhydrophobic Surfaces. *Nanoscale Res. Lett.* **2016**, *11*, 231. [CrossRef] [PubMed]
20. Liu, F.C.; Hao, Y.S.; Wang, Z.Y.; Shi, H.W.; Han, E.H.; Ke, W. Flaking and degradation of polyurethane coatings after 2 years of outdoor exposure in Lhasa. *Chin. Sci. Bull.* **2010**, *55*, 650–655. [CrossRef]
21. Golczak, S.; Kanciurzewska, A.; Fahlman, M.; Langer, K.; Langer, J.J. Comparative XPS surface study of polyaniline thin films. *Solid State Ion.* **2008**, *179*, 2234–2239. [CrossRef]
22. Radhakrishnan, S.; Siju, C.R.; Mahanta, D.; Patil, S.; Madras, G. Conducting polyaniline-nano-TiO_2 composites for smart corrosion resistant coatings. *Electrochim. Acta* **2009**, *54*, 1249–1254. [CrossRef]
23. Pour-Ali, S.; Dehghanian, C.; Kosari, A. In situ synthesis of polyaniline-camphorsulfonate particles in an epoxy matrix for corrosion protection of mild steel in NaCl solution. *Corros. Sci.* **2014**, *85*, 204–214. [CrossRef]
24. Wang, Z.B.; Wang, Z.Y.; Hu, H.X.; Liu, C.B.; Zheng, Y.G. Corrosion Protection Performance of Nano-SiO_2/Epoxy Composite Coatings in Acidic Desulfurized Flue Gas Condensates. *J. Mater. Eng. Perform.* **2016**, *25*, 3880–3889. [CrossRef]
25. Sridhar, T.M.; Mudali, U.K.; Subbaiyan, M. Preparation and characterisation of electrophoretically deposited hydroxyapatite coatings on type 316L stainless steel. *Corros. Sci.* **2003**, *45*, 237–252. [CrossRef]
26. Zhang, H.; Yao, G.C.; Wang, S.L.; Liu, Y.H.; Luo, H.J. A chrome-free conversion coating for magnesium-lithium alloy by a phosphate-permanganate solution. *Surf. Coat. Technol.* **2008**, *202*, 1825–1830. [CrossRef]
27. Ruhi, G.; Bhandari, H.; Dhawan, S.K. Designing of corrosion resistant epoxy coatings embedded with polypyrrole/SiO_2 composite. *Prog. Org. Coat.* **2014**, *77*, 1484–1498. [CrossRef]

28. Shen, G.X.; Chen, Y.C.; Lin, L.; Lin, C.J.; Scantlebury, D. Study on a hydrophobic nano-TiO_2 coating and its properties for corrosion protection of metals. *Electrochim. Acta* **2005**, *50*, 5083–5089. [CrossRef]
29. Milosev, I.; Jovanovic, Z.; Bajat, J.B.; Jancic-Heinemann, R.; Miskovic-Stankovic, V.B. Surface Analysis and Electrochemical Behavior of Aluminum Pretreated by Vinyltriethoxysilane Films in Mild NaCl Solution. *J. Electrochem. Soc.* **2012**, *159*, C303–C311. [CrossRef]
30. Liu, C.; Bi, Q.; Leyland, A.; Matthews, A. An electrochemical impedance spectroscopy study of the corrosion behaviour of PVD coated steels in 0.5 N NaCl aqueous solution: Part II. EIS interpretation of corrosion behaviour. *Corros. Sci.* **2003**, *45*, 1257–1273. [CrossRef]
31. Liu, X.W.; Xiong, J.P.; Lv, Y.W.; Zuo, Y. Study on corrosion electrochemical behavior of several different coating systems by EIS. *Prog. Org. Coat.* **2009**, *64*, 497–503. [CrossRef]
32. Yan, M.C.; Vetter, C.A.; Gelling, V.J. Corrosion inhibition performance of polypyrrole Al flake composite coatings for Al alloys. *Corros. Sci.* **2013**, *70*, 37–45. [CrossRef]
33. Hirayama, R.; Haruyama, S. ELECTROCHEMICAL IMPEDANCE FOR DEGRADED COATED STEEL HAVING PORES. *Corrosion* **1991**, *47*, 952–958. [CrossRef]
34. Kouisni, L.; Azzi, M.; Dalard, F.; Maximovitch, S. Phosphate coatings on magnesium alloy AM60 Part 2: Electrochemical behaviour in borate buffer solution. *Surf. Coat. Technol.* **2005**, *192*, 239–246.
35. Cubides, Y.; Castaneda, H. Corrosion protection mechanisms of carbon nanotube and zinc-rich epoxy primers on carbon steel in simulated concrete pore solutions in the presence of chloride ions. *Corros. Sci.* **2016**, *109*, 145–161. [CrossRef]
36. Singh, A.; Ahamad, I.; Singh, V.K.; Quraishi, M.A. Inhibition effect of environmentally benign Karanj (Pongamia pinnata) seed extract on corrosion of mild steel in hydrochloric acid solution. *J. Solid State Electrochem.* **2011**, *15*, 1087–1097. [CrossRef]
37. Hirschorn, B.; Orazem, M.E.; Tribollet, B.; Vivier, V.; Frateur, I.; Musiani, M. Determination of effective capacitance and film thickness from constant-phase-element parameters. *Electrochim. Acta* **2010**, *55*, 6218–6227. [CrossRef]
38. Su, X.M.; Zhou, Q.; Zhang, Q.Y.; Zhang, Y.; Zhang, H. Study on the deterioration process of bipolar coating using electrochemical impedance spectroscopy. *Appl. Surf. Sci.* **2011**, *257*, 6095–6101. [CrossRef]
39. Zhou, C.L.; Lu, X.; Xin, Z.; Liu, J. Corrosion resistance of novel silane-functional polybenzoxazine coating on steel. *Corros. Sci.* **2013**, *70*, 145–151. [CrossRef]
40. Castela, A.S.L.; Simoes, A.M.; Ferreira, M.G.S. EIS evaluation of attached and free polymer films. *Prog. Org. Coat.* **2000**, *38*, 1–7. [CrossRef]
41. Yun, H.; Li, J.; Chen, H.B.; Lin, C.J. A study on the N-, S- and Cl-modified nano-TiO_2 coatings for corrosion protection of stainless steel. *Electrochim. Acta* **2007**, *52*, 6679–6685. [CrossRef]
42. Mansfeld, F. MODELS FOR THE IMPEDANCE BEHAVIOR OF PROTECTIVE COATINGS AND CASES OF LOCALIZED CORROSION. *Electrochim. Acta* **1993**, *38*, 1891–1897. [CrossRef]
43. Hassan, H.H.; Abdelghani, E.; Amin, M.A. Inhibition of mild steel corrosion in hydrochloric acid solution by triazole derivatives—Part I. Polarization and EIS studies. *Electrochim. Acta* **2007**, *52*, 6359–6366. [CrossRef]
44. Tang, N.; vanOoij, W.J.; Gorecki, G. Comparative EIS study of pretreatment performance in coated metals. *Prog. Org. Coat.* **1997**, *30*, 255–263. [CrossRef]
45. Liu, J.G.; Gong, G.P.; Yan, C.W. EIS study of corrosion behaviour of organic coating/Dacromet composite systems. *Electrochim. Acta* **2005**, *50*, 3320–3332.